Experimental characterization and modeling of the temperature and rate-dependent shear behaviour of powder-impregnated glass fiber/PA66 woven semipregs

Theo Baumard, Gary Menary, Olivier de Almeida, Peter Martin, Fabrice
Schmidt, Jérôme Bikard

▶ To cite this version:

HAL Id: hal-02134092
https://imt-mines-albi.hal.science/hal-02134092

Experimental characterization and modeling of the temperature and rate-dependent shear behaviour of powder-impregnated glass fiber/PA66 woven semipregs

Théo Baumard[a,b], Gary Menary[a], Olivier De Almeida[b,*], Peter Martin[a], Fabrice Schmidt[b], Jérôme Bikard[c]

[a] *School of Mechanical and Aerospace Engineering, Queen's University Belfast, Belfast, Northern Ireland, BT9 5AH, United Kingdom*
[b] *Institut Clément Ader (ICA), Université de Toulouse, CNRS, Mines Albi, UPS, INSA, ISAE-SUPAERO, Campus Jarlard, 81013, Albi, CT Cedex 09, France*
[c] *Solvay R&I, 85 rue des Frères Perret, 69192, Saint Fons, France*

ABSTRACT

This study focuses on the characterization of the in-plane shear response of a novel powder-impregnated, non-consolidated PA66/glass semipreg to evaluate its forming behaviour. The effects of temperature and rate on the behaviour of the semipreg and the preconsolidated material were investigated using bias-extension tests. Results obtained show an increase in shear stress with decreasing temperature and increasing rate, with the semipreg exhibiting a lower sensitivity to the test speed. An increase of the flow distance to impregnate the yarns, due to intra-ply sliding mechanisms specific to the powder-impregnated semipreg, is observed. A model based on a hypoelastic approach with temperature and rate dependence is proposed to represent the material behaviour. Isothermal simulations of the bias-extension test are conducted. Results show a good agreement between the model and experimental data in terms of force and shear angle prediction.

1. Introduction

The use of thermoplastic composites in structural parts is growing in the automotive industry, as compliance with stricter CO_2 emissions regulations ($95\,g\,km^{-1}$ by 2020 in the EU, $91\,g\,km^{-1}$ by 2025 in the USA [1]) is pushing the need for lighter structural frame and body parts. To reach the production rates required by this high-volume market, manufacturing processes allowing for short cycle times ($< 1min$) such as thermoforming have to be used [2]. This process consists of heating a pre-consolidated blank of thermoplastic composite in an infrared oven above the melting temperature of the matrix; the blank is then transferred into a press where it is stamped to shape [3,4].

A potential way of reducing the costs associated with this process would be to form directly from non-consolidated preforms, thus removing the need for a preliminary consolidation step. This approach is made especially viable with the recent development of semipreg materials (powder-impregnated, commingled) that reduce the distance needed to impregnate the yarns [5], and new formulation of thermoplastic polymers presenting a low melt viscosity that allow for consolidation with pressures as low as 0.15 MPa [6]. Optimizing the thermoforming of double curvature parts for these materials requires an understanding of both the mechanical behaviour during the forming phase (where in-plane shear is the principal mode of deformation [7]) and the impregnation behaviour during the compaction and re-consolidation.

Most of the work related to direct forming of semipregs has been focused on commingled composites, and especially on consolidation [8]. Bernet et al. [9,10] proposed a model allowing for the prediction of residual void content in non-isothermal stamp forming of non-consolidated, unidirectional commingled yarn fabrics into flat panels, based on the impregnation of a single representative yarn. Thomann et al. [11,12] investigated the forming of flat laminates from non-consolidated PA12-and PBT-carbon fibre commingled yarns, showing the importance of the commingling quality on the resulting void content.

Studies published in 2006 [13,14] have shown the viability of forming more complex parts (either non-developable or developable) from unconsolidated woven commingled fabric, showing good mechanical properties even when compared to their pre-consolidated counterparts.

Fewer studies have been focused on the use of powder-impregnated semipregs, where the matrix is deposited with a wet or dry process

---

* Corresponding author.
E-mail address: olivier.dealmeida@mines-albi.fr (O. De Almeida).

either on the tows before weaving (powder coated towpregs) or directly on the fabric after weaving. This class of semipreg has the advantage of being easier to handle as the matrix distribution stabilizes the fabric: the thermoplastic powder effectively acts as a binder on the dry fabric, preventing fraying and displacement of the yarns during the cutting and kitting operations. The drapability at room temperature is however greatly impeded. Connor et al. [15] used both commingled fabrics and powder coated towpregs to form corrugated sheets with high processing rates, resulting in parts with void volume fraction < 2% in both cases. Even though the commingled material required a higher processing temperature to reach this void content, the comparison between the two precursor types is biased by variations in the viscosity of the PA12 grades used.

Several authors have investigated and modelled the shear behaviour of preconsolidated woven thermoplastic composites [16–19] or commingled fabrics [20–22], showing the influence of the thermo- and rate-dependent behaviour of the matrix on the shear response. Despite the intense work in the field of forming of thermoplastic composites, no studies have yet addressed the shear behaviour of non-consolidated powder-impregnated woven fabrics, which is primordial for accurate process simulation.

This paper presents an experimental study on the shear behaviour of a powder-impregnated PA66/glass woven semipreg in a range of temperature and shear rate relevant to the thermoforming process. The aim of this work is to characterize the shear behaviour of the material and its dependence on temperature and rate, in its as-received configuration and after a preconsolidation step. A full-factorial bias-extension test program is conducted; experimental data obtained for the consolidated and non-consolidated material are presented and compared in terms of shear rate and temperature effect. The ability of a hypoelastic approach with a multiplicative decoupling shear model to represent the behaviour of the semipreg material is assessed.

2. Material

The material used in this study is a twill 2/2 woven glass fabric, powder-impregnated with polyamide 66 (PA66) and provided by Solvay. The main characteristics of the fabric are listed in Table 1. The matrix used is a high fluidity PA66, with a dynamic melt viscosity of 30–50 Pa s at $10s^{-1}$ [23]. In its as-received state, the matrix is distributed as a network of semi-coalesced droplets on both faces of the fabric, as shown in the micrographs of Figs. 1 and 2.

In contrast with classical powder-impregnation techniques where the matrix is deposited on fiber tows via solution/slurry processing or dry powder impregnation [24], the deposition process is conducted after the weaving operation which helps to reduce the material costs, as no adaptations are required for the loom; the matrix distribution is, however, highly heterogeneous through the thickness of the fabric.

A DSC analysis performed at 20°C/min and presented in Fig. 3 shows a melting temperature of 260°C and a crystallization temperature of 225°C. In the industrial process, the blank is usually preheated up to 30°C above the melting temperature of the matrix to take into account the convective cooling during the transfer phase from the heating station to the forming station. The relevant thermoforming window for

Table 1
Main material characteristics.

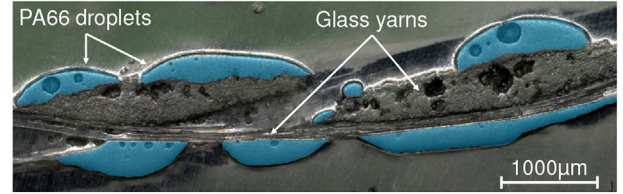| Matrix	PA66
Fibers	E-glass
Weave type	Twill 2/2
Warp/weft ratio	Balanced
Semipreg style	Powder, 2 faces
Areal weight (glass fabric)	600 g m^{-2}
Areal weight (semipreg)	960 g m^{-2}
v_f (consolidated)	50/52%

Fig. 1. Cross-section micrograph (x50) of the non-consolidated semipreg material, showing warp and weft yarns with polyamide droplets (highlighted in blue). (For interpretation of the references to colour in this figure legend, the reader is referred to the Web version of this article.)
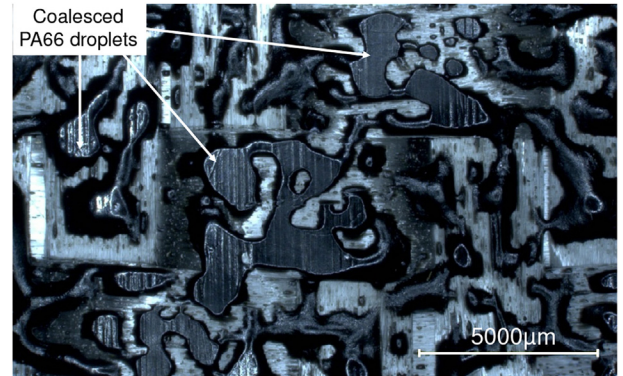

Fig. 2. Surface micrograph of the non-consolidated semipreg, showing the network of coalesced polyamide droplets.
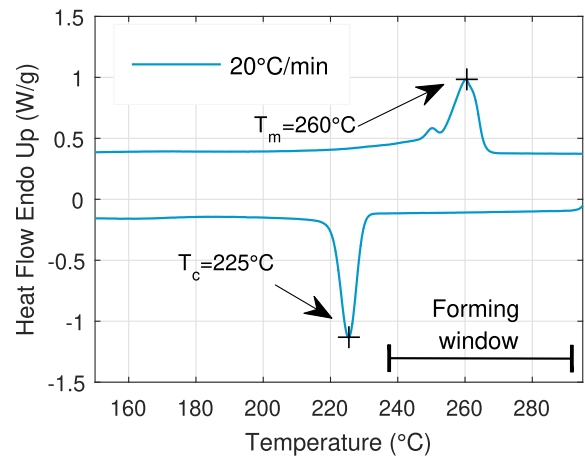

Fig. 3. DSC analysis: heating/cooling at 20°C, showing the processing temperature window.

this material can therefore be considered to be between 235°C and 295°C.

2.1. Consolidation

To serve as a reference when comparing with the as-received material, single plies of $320 \times 300mm^2$ with a $\pm 45°$ orientation were thermocompressed at 295°C under 2 bar for 5min in a 1000 kN press equipped with an induction heated flat mould. The resulting consolidated plates present a thickness of 0.51 ± 0.02 mm.

3. Experimental procedure

3.1. Bias-extension test

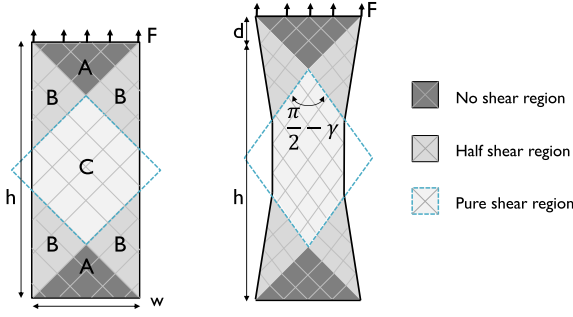The bias-extension test is a well established test for the

Fig. 4. Kinematics of the bias-extension test. Initial (left) and deformed (right) sample, showing the non-homogeneous shear stress field.

characterization of in-plane shear for woven fabrics, in which a rectangular sample of aspect ratio greater than 2 is subjected to tensile loading, the initial orientation of the fabric being at 45° relative to the load direction. The kinematics of the test are presented in Fig. 4: as yarns in the central region of the sample are not clamped, and assuming no slippage between the warp and weft directions, the central region is in a state of pure shear [7,22]. As the region closer to the grips does not contribute to the force measured during the test, the bias-extension test also presents the advantage of being less sensitive to temperature gradients due to the sample cooling from the grips when compared to the picture frame test [19] (although modifications to the sample geometry or picture frame grips can greatly mitigate these effects [25]).

3.2. Experimental set-up

Single ply samples of height $h = 250$ mm and width $w = 100$ mm were cut out of the semipreg and the preconsolidated plates. The specimens were marked with high-temperature paint to facilitate the post-processing of the shear angle evolution. To minimize the influence of moisture on the behaviour of the matrix, all specimens were dried at 80°C for 12 h as per the manufacturer recommendation prior to testing. The bias-extension tests were conducted using a MTS 250 kN servo-hydraulic machine equipped with a 5 kN load cell and a MTS651 environmental chamber. The accuracy of the load cell at small loads has been verified with weights between 5N and 100N. Results show the systematic error and random error below 5% and 10% at 5N respectively, and below 2.5% and 5% for loads above 10N. Purpose-made grips described in Fig. 5 were used to prevent slippage of the samples. To ensure proper clamping of the sample above melting temperature, the grip force is introduced by a combination of set screws and compression springs. Each test was filmed with an Allied Vision AVT Pike camera to track the evolution of shear angle during the deformation.

To replicate the thermal history seen by the blank in the industrial thermoforming process, the samples were heated to 295°C before being cooled down to the test temperature. The temperature homogenization
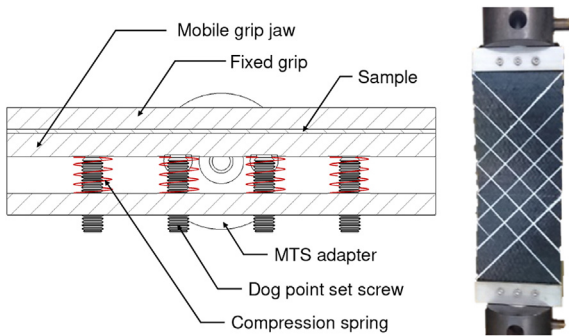

Fig. 5. Grips used for the bias extension tests. Left: top view drawing, right: preconsolidated sample mounted in the grips.
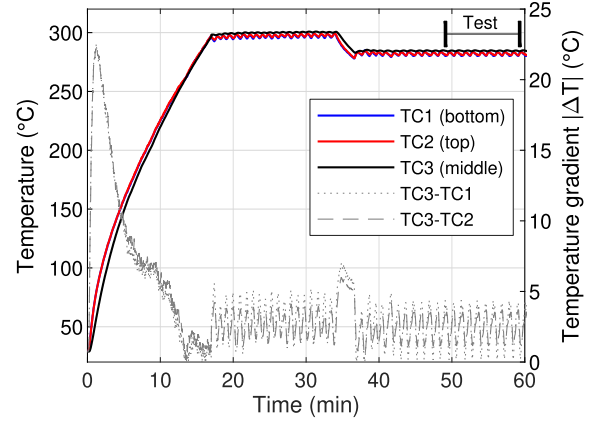

Fig. 6. Thermal cycle applied to the sample prior to testing. Thermocouples are located at the middle of the sample and half-height of the top and bottom non-sheared regions; dotted lines represent the absolute values of temperature gradients.

steps were kept intentionally short (15min) to limit the thermal oxidation of the PA66. Convection and grips-induced temperature gradients were evaluated prior to testing with thermocouples distributed along the length of the sample (see Fig. 6). A thermal probe consisting of a type-K thermocouple held in between two plies of the material (as proposed in Ref. [26]) was used to monitor the temperature during testing.

A full factorial experiment with two temperatures in the processing range (265°C and 280°C) and three different speeds (10, 100 and 1000 mm/min) was conducted for each material (semipreg and preconsolidated). A minimum of three samples were tested per test condition. For the sake of completeness, bias-extension tests were also conducted on the dry twill fabric at room temperature and 10 mm/min.

3.3. Post-processing procedure

As the determination of the shear angle through geometric considerations does not lead to valid results after the onset of sliding [7], an optical method was used. The images obtained during the test were post-processed using routines developed in ImageJ [27] and MATLAB: the shear angle is calculated as the average on three discrete measurements in the central region of the sample as shown in Fig. 7.

Shear force was determined from axial load using the energetic approach presented by Launay et al. [28], and subsequently reviewed in Ref. [29], where the power related to the displacement of the grips is equated with the power needed to shear the different regions of the sample:

$$F_{sh} = \frac{1}{(2h - 3w)\cos\gamma}\left(\left(\frac{h}{w} - 1\right)F\left(\cos\frac{\gamma}{2} - \sin\frac{\gamma}{2}\right) - wF_{sh}\left(\frac{\gamma}{2}\right)\cos\frac{\gamma}{2}\right)$$

(1)

where F_{sh} is the normalised shear force, F the axial force as recorded during the test, γ the shear angle and h and w the sample initial height and width, respectively (see Fig. 4 for reference). As the shear force is obtained recursively from the shear force at the half shear angle, linearity is assumed at the initial step of the computation:

$$F_{sh}\left(\frac{\gamma}{2}\right) = \frac{F_{sh}(\gamma)}{2}$$

(2)

The Cauchy shear stress, assuming the material as a continuous medium, is then calculated by dividing by the initial sample thickness [30].
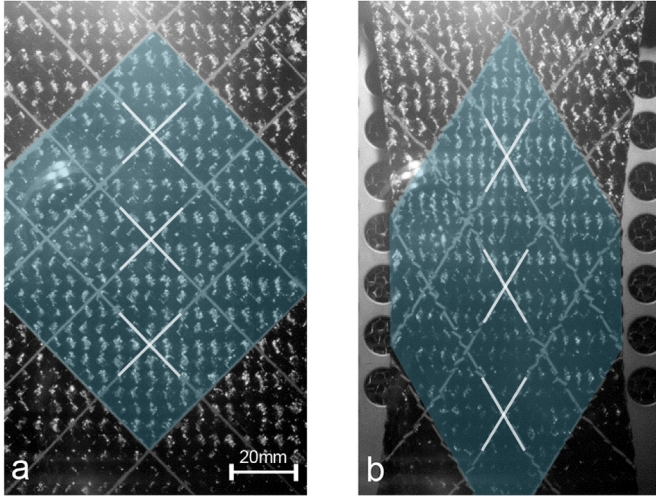
Fig. 7. Preconsolidated sample in (a) undeformed configuration and (b) after 30 mm of extension at 265°C and 1000 mm/min, with location of the shear angle measurements. The central region undergoing pure shear is highlighted in blue. (For interpretation of the references to colour in this figure legend, the reader is referred to the Web version of this article.)

4. Results

The axial force versus extension curves obtained are presented in Fig. 8 for all test repeats on the semipreg material at 265°C. The mean force at each test speed is shown with solid lines, with grey surfaces representing the standard deviation. The reproducibility of the tests is good, with standard deviation increasing up to a maximum of 20% after the onset of sliding (when the specimen is failing).

The resulting shear stress versus shear angle curves are shown in Figs. 9 and 10 for the preconsolidated and semipreg material respectively. The curves present the same features regardless of the test conditions: the sample first undergoes a realignment in the plane (as the heating cycle induces sag). No change in shear angle was observed as the material became slack from heating, which indicates that the sag was accommodated by buckling rather than shearing of the sample. As proposed by Harrison [19], the measured displacement data were shifted by approximately 1 mm to account for this effect. Static friction initially prevents shearing until the applied load is sufficient; at small shear angles, the yarns are free to rotate around their crossover points and the shear stress arises from inter-yarn friction only. As the yarns gradually come in contact, transverse compaction leads to a gradual increase in the shear stiffness. The theoretical asymptote of the curve corresponding to the compaction limit of the yarns is not reached, as
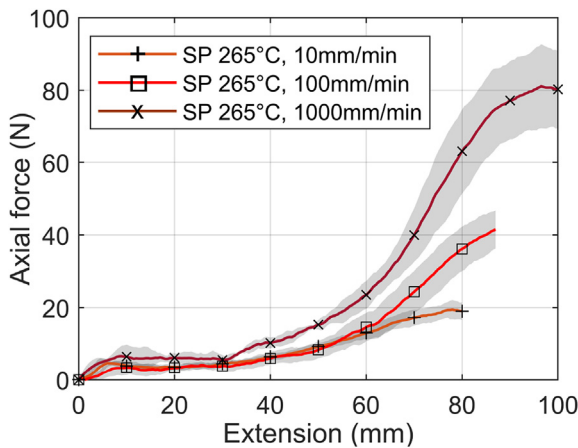

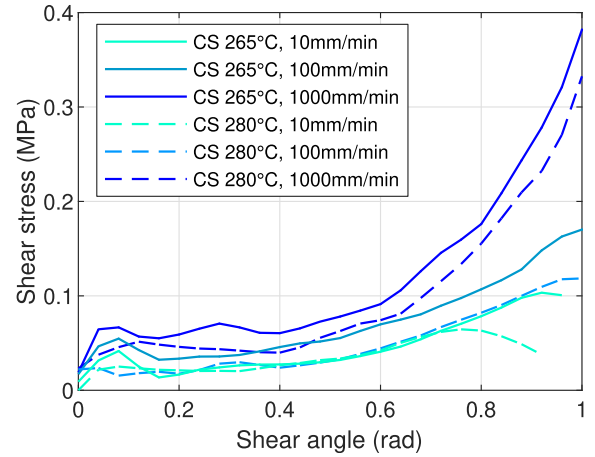**Fig. 8.** Axial force versus extension curves; semipreg material (SP) at 265°C.

Fig. 9. Average shear stress versus shear angle curves for preconsolidated specimens (CS). Solid and dashed lines represent tests at 265°C and 280°C respectively.
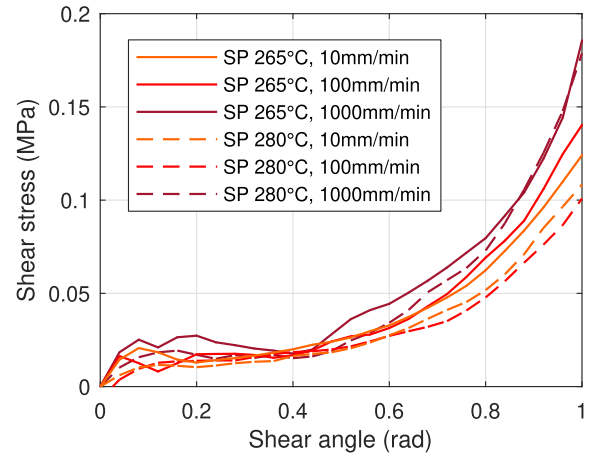

Fig. 10. Average shear stress versus shear angle curves for semipreg specimens (SP). Solid and dashed lines represent the test at 265°C and 280°C respectively.

intra-ply slippage mechanisms (crossover and inter-tow slip) become the primary mode of deformation to accommodate the prescribed displacement [19].

Intra-yarn shear is also observed during the deformation, as can be seen in Fig. 11 where lines drawn on the undeformed sample present a loss of continuity due to the rotation of segments on yarns initially orthogonal to the lines. The low values of maximum shear stresses recorded here are attributed to the fabric coarseness (2.6 ends per cm) and weave style which reduces the waviness and affect the inter-yarn friction behaviour as reported by Dong et al. [31].

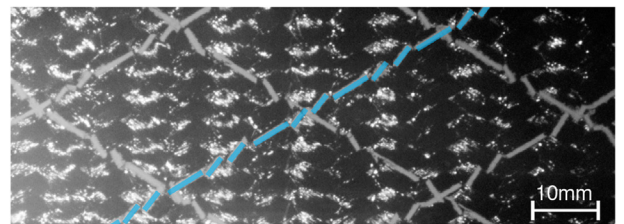Additional comparison between results for both the preconsolidated

Fig. 11. Detail of a preconsolidated sample at 265°C, 1000 mm/min after 30 mm of extension, with an initially continuous and straight line showing intra-yarn shear (highlighted in blue). (For interpretation of the references to colour in this figure legend, the reader is referred to the Web version of this article.)
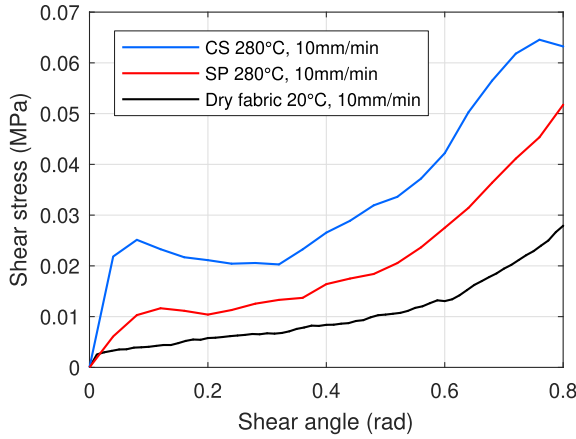
Fig. 12. Average shear stress versus shear angle curves for the preconsolidated (CS, blue) and semipreg (SP, red) specimens at 280°C, and dry fabric at room temperature and 10 mm/min. (For interpretation of the references to colour in this figure legend, the reader is referred to the Web version of this article.)

and semipreg composite and the dry fabric at 10 mm/min are presented in Fig. 12: the stiffening effect of the matrix is clearly visible, with values of shear stress for the dry fabric being on average 50% and 30% of the semipreg and preconsolidated material respectively.

4.1. Temperature effect

The tests conducted at 280°C and 265°C show an increase of the measured shear stress with decreasing temperature for both the pre-consolidated and semipreg material. Fig. 13 presents the relative effect on shear stress of: (a) decreasing the temperature from 280°C to 265°C and (b) increasing the test speed by 1 or 2 decades, averaged for shear angles between 0.1 rad and 0.8 rad to ignore both the initial static friction and the sliding phase. The consolidated and semipreg material are denoted by blue and red bars respectively. Temperature is shown to have a significant effect on the observed behaviour, with the exception of tests conducted on the preconsolidated material at 10 mm/min, for which the only noticeable difference is the onset of sliding (see Fig. 9). The effect of temperature on the shear behaviour of woven composites is well documented in the literature [17,25,32], and is attributed to the increase in viscosity of the thermoplastic matrix as the material cools from the melt. A higher viscosity at lower temperatures impedes the shearing of the yarns that are either fully impregnated (in the case of the preconsolidated fabric) or sandwiched between polymer rich layers (in the case of the semipreg).

4.2. Rate effect

Strain rate dependence is not as widely reported as temperature dependence [25,33], and as a result is not taken into account as often in modeling approaches [7]. The average effect on the shear stress of increasing the test speed is shown in Fig. 13b. In the case of the pre-consolidated composite (blue bars), an increase in the strain rate leads to a significant increase of the shear stress with exception of the tests conducted at 280°C and 100 mm/min. Higher shear angles before sliding are also achieved at higher speedsas observed in Fig. 9. In the case of the semipreg, increasing the test speed from 10 to 100 mm/min does not have a significant effect, withonly tests at 1000 mm/min presenting a slight increase in the observed shear stress.

4.3. Sliding behaviour

Sixteen tests were conducted up to an extension of 150 mm to observe the behaviour of the samples past the onset of sliding. In the case of semipreg samples where the matrix is located only on the top and bottom surfaces of the fabric, cross-over slip leads to a characteristic pattern of visually resin-free macroscopic zones and accumulation of resin at the boundaries of these zones (see Fig. 14). This behaviour is assumed to be due to a combination of non-coated surfaces becoming exposed and resin accretion in the region of yarn crossover opposite to the direction of sliding. Since the resin is distributed uniformly in the preconsolidated material, the effect is limited to semipreg samples. The maximum polymer flow distance to impregnate the yarns can be increased by one order of magnitude; the modification of the local matrix volume fraction can lead to dry spots after the consolidation of the part which is detrimental to the resulting mechanical properties.

5. Modeling

Various approaches have been proposed in the recent literature to model and simulate the behaviour of woven composites during forming. Discrete approaches have been presented at the microscale [34] or mesoscale [35] for the draping of dry fabrics; although they allow for the prediction of loss of cohesion of the fabric or fiber/yarn pull-out, the computational costs associated with the high number of contact interactions considered limit their use to the simulation of a few unit cells. Even though the assumptions made are not valid at small scales, semi-discrete or continuous approaches are more widely used [36–38] within hyper- or hypoelastic frameworks suited to analysis at large strains. These approaches allow to take into account the effect of the viscous matrix in constitutive laws without explicitly modeling it, and recent studies have been successful in simulating the temperature and rate dependent behaviours of preconsolidated composites during forming [17,18]. The approach used here is an extension of the model presented by Pierce [39] and based on previous work by Khan [40] and Peng [41]. The model is based on a hypoelastic formulation:

$$\sigma^{\nabla} = \boldsymbol{C} : \boldsymbol{D} \tag{3}$$

where σ is the Cauchy stress tensor, $\boldsymbol{D}$ the strain rate tensor and $\boldsymbol{C}$ a fourth-order constitutive tensor expressed here in the frame of the fibers. $^{\nabla}$ denotes an objective derivation operator ensuring the absence of
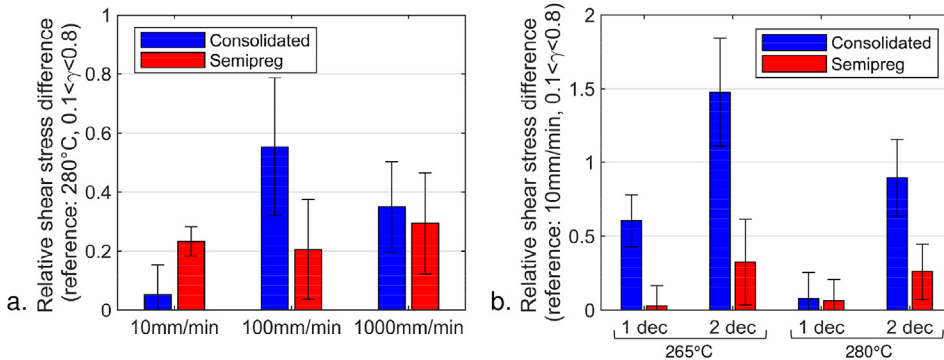

Fig. 13. Average relative shear stress difference resulting from: (a) reducing the temperature by 15°C, (b) increasing the speed by 1 or 2 decades for the preconsolidated (blue) and semipreg (red) specimens. (For interpretation of the references to colour in this figure legend, the reader is referred to the Web version of this article.)
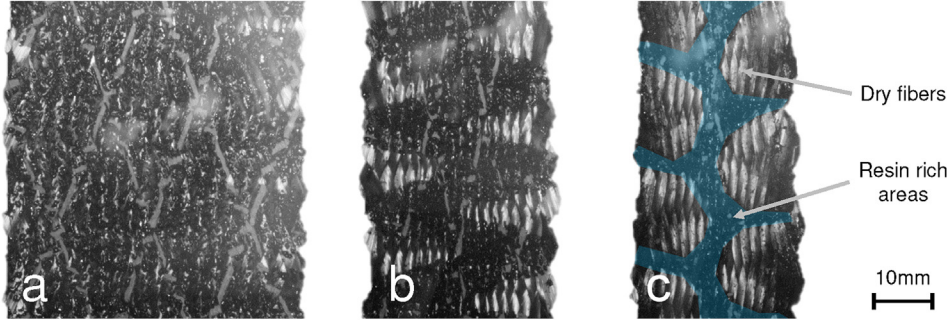
Fig. 14. Semipreg sample at 280°C, 1000 mm/min after (a) 60 mm, (b) 100 mm and (c) 140 mm of extension, showing the onset of slippage and characteristic pattern of resin-rich areas highlighted in blue. (For interpretation of the references to colour in this figure legend, the reader is referred to the Web version of this article.)

spurious stresses from rigid body rotations. Two orthogonal frames fixed with the fibers directions are constructed and updated using the deformation gradient tensor $\boldsymbol{F}$. Commercial finite elements softwares make use of Jaumann or Green-Naghdi formulations, which are based on average material rotations (from polar decomposition of the deformation gradient, or rotation of the corotational frame). The strains computed in these frames need to be expressed in the fiber axes before the constitutive law can be applied. The resulting stress increments are accumulated in each fiber frame using a mid-point integration before being summed in the current working frame. Considering elastic tensile terms E_1 and E_2 and shear modulus G_{12} only, the constitutive law in fiber direction α is then expressed as:

$$
\begin{bmatrix} d\boldsymbol{\sigma}_{11}^{f_\alpha} \\ d\boldsymbol{\sigma}_{22}^{f_\alpha} \\ d\boldsymbol{\sigma}_{12}^{f_\alpha} \end{bmatrix} = \begin{bmatrix} \delta_{\alpha 1}E_1 & 0 & 0 \\ 0 & \delta_{\alpha 2}E_2 & 0 \\ 0 & 0 & G_{12} \end{bmatrix} \begin{bmatrix} d\boldsymbol{\varepsilon}_{11}^{f_\alpha} \\ d\boldsymbol{\varepsilon}_{22}^{f_\alpha} \\ d\boldsymbol{\varepsilon}_{12}^{f_\alpha} \end{bmatrix}
$$

(4)

where $\delta_{\alpha i}$ is the Kronecker delta function. The temperature and rate-dependence is assumed to be related only to the in-plane shear term and tension/shear couplings are neglected (although recent work has shown that tension in the yarns can affect the shear response through an increase of the contact forces at crossover points [42]; an uncoupled model is however sufficient to predict the shear deformation patterns [43]). The analytical expression of the shear modulus developed by Machado et al. [32] for preconsolidated composites is used to represent the nonlinear, temperature and rate-dependent shear behaviour. This empirical model assumes a multiplicative decoupling between the different effects (eq. (5)).

$$
G_{12}(\gamma, \dot{\gamma}, T) = (a_1 + 2a_2\gamma + 3a_3\gamma^2)\left(1 + \left(\frac{\dot{\gamma}}{D}\right)^{\frac{1}{P}}\right)\left(e^{A\frac{T-T_0}{T_0}}\right)
$$

(5)

where a_1, a_2 and a_3 are fit coefficients of the shear stiffness, D and P are parameters of Cowper-Symonds overstress law [44], and T_0 and A are the reference temperature and temperature scaling factor respectively.

The model parameters have been determined by minimizing the sum of least square errors associated with each shear stress versus shear angle/shear rate experimental curve. The specificities of the bias-extension test lead to a variable shear rate, which was therefore evaluated by numerical differentiation of the shear angle using finite differences. The optimization problem was solved using an interior-point algorithm in MATLAB [45]. The resulting parameters are presented in Table 2, and Figs. 15 and 16 show the superposition of the model prediction and average experimental curves in the shear angle/shear rate plane for the preconsolidated and semipreg composite respectively. The sum of squared relative residuals for each configuration, divided by the corresponding number of data points, is presented in Fig. 17. The model provides a correct description of the behaviour in both cases, including the lower sensitivity of the semipreg to temperature and rate as can be seen in the values of the temperature scaling factor and exponent of the Cowper-Symonds law.

Table 2
Material model parameters.

Parameter	Preconsolidated	Semipreg
a_1 (MPa)	0.3351	0.3276
a_2 (MPa)	-0.9356	-0.9040
a_3 (MPa)	0.8466	0.8817
D (rad s^{-1})	2.7251×10^{-3}	5.7215×10^{-3}
P ($-$)	3.6578	7.4378
A ($-$)	-6.9429	-10.6933
T_0 (K)	495.01	499.97

The model has been implemented in Abaqus/Explicit by means of a VUMAT user subroutine. Isothermal bias-extension simulations were conducted to validate the model at various temperatures. Under-integrated shell elements with temperature degree of freedom and approximate size of 7×7 mm^2 were used; to avoid numerical tension locking issues described by Hamila and Boisse [46], the mesh has been aligned with the initial warp and weft yarn directions.

Fig. 18 presents the simulated shear angle distribution in a preconsolidated sample at different temperatures, at an extension of 30 mm. The different zones predicted by the theory are clearly defined. The maximum value of simulated shear angle is increasing at higher temperatures, as the shear stiffness of the material decreases; this is also shown in the case of forming simulations [16]. The simulated axial force required to stretch the sample during the test is plotted in Fig. 19 at 1000 mm/min. The axial force is underestimated at low shear angles ($\gamma < 0.1$ rad), as the fit function used in the model does not reproduce the sharp increase in axial force observed at the transition between the static and kinetic friction regimes. At high shear angles, the simulation predicts a higher axial force than measured experimentally. The effect of temperature on the measured force is however accurately reproduced. The error between simulation and experimental shear angle measurement is plotted in Fig. 20 for a variety of configurations. The simulation overestimates the shear angle in all cases and the error increases noticeably at higher extension, up to a value of 10° at 65 mm. These differences are partly due to the inability of the continuous approach used in representing the locking and subsequent sliding of the discrete yarns.

6. Discussion

The experimental test campaign has outlined differences in the shear behaviour of the preconsolidated and semipreg composites, the latter presenting a lower dependence on the test temperature and virtually no dependence on the shear rate. These differences are likely due to the spatial distribution of the resin within the woven reinforcement, as other parameters are kept identical. The stresses generated during the in-plane shear of woven fabrics are due initially to inter-yarn friction and at large shear angles to transverse compression [47]. In the case of single preconsolidated plies sheared at high temperatures, the
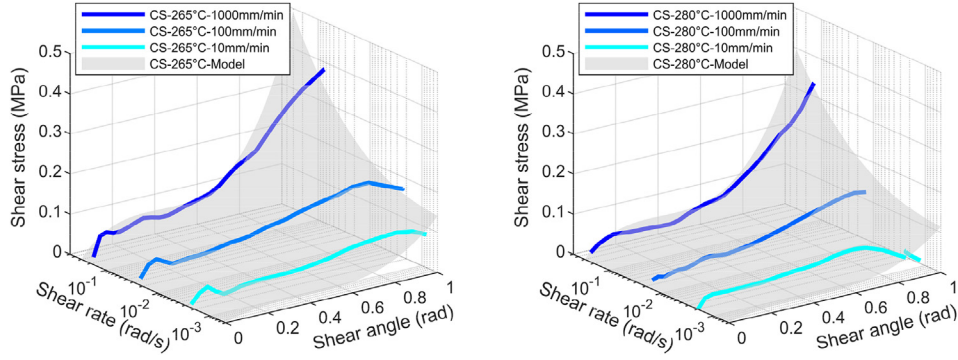
Fig. 15. Comparison between experimental data and model for preconsolidated specimens (CS) at 265°C (left) and 280°C (right). The grey surface represent the model prediction.

thermoplastic matrix has two competitive effects: it decreases inter-tow friction by acting as a lubricant, but its viscosity also restricts the macroscopic movements of the yarns in a rate-sensitive fashion [48,49]. This behaviour is consistent with the results presented here with a stiffening of the shear response at higher testing speeds, and corroborated by results on temperature and rate dependent fabric/fabric lubricated friction coefficients presented in the literature [50–52].

In the case of the semipreg, the matrix is present only on the apparent surfaces of the woven fabric and the yarn crossover points are dry. The evolution of friction coefficients for dry fabric/fabric, fabric/tool or yarn/yarn as a function of velocity has been extensively studied, in a variety of test conditions. Results presented by Liu et al. [53] for parallel and orthogonal yarns show an increase of the yarn/yarn friction coefficient at small sliding speeds and a slight decrease at larger speeds, with higher coefficients for parallel yarns, which is also shown in Ref. [54]. Results of a benchmark study on commingled fabric/tool friction [55] show no statistical effect of the velocity at room temperature (dry friction), while the friction coefficient is shown to increase with increasing velocity at temperature above the melting point of the considered matrix. Recent work from Montero et al. [56] on yarn/yarn friction reports no effect of the velocity in the case of parallel yarns, and a slight increase in orthogonal yarns. These findings are coherent with the results obtained for the semipreg which show a limited effect of the shear rate. The absence of statistical difference observed here between tests on the consolidated material at 10 mm/min, 265°C and 100 mm/min, 265°C, and between tests on the semipreg at 10 mm/min and 100 mm/min can potentially be explained by the dispersion induced by the high capacity of the load cell compared to the measured axial forces.

The phenomenological model used allows for a correct quantitative representation of the material behaviour. The deviations observed might be caused by effects unaccounted for in the model such as a potential coupling between the effects of temperature and shear rate,
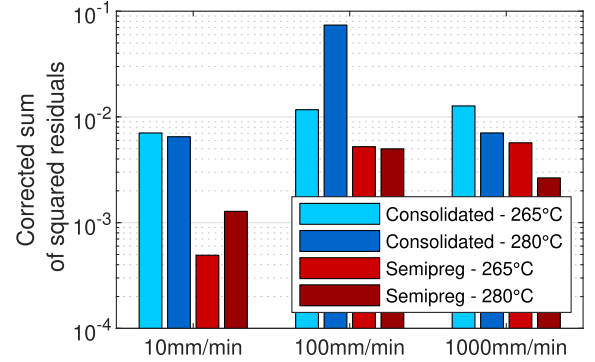

Fig. 17. Sum of squared relative residuals corrected by number of data points in each configuration.

characterization induced errors due to the normalisation method employed [57], or by the limitations of the continuous approach which is unable to properly replicate the slippage mechanisms, especially in the case of the semipreg.

Additional problematics have to be considered to propose a comprehensive simulation approach for the direct forming of non-consolidated semipreg, as both the infrared heating phase and the impregnation/reconsolidation will involve different mechanisms. The matrix droplets at the surface of the fabric lead to thermal contact resistances that increase temperature gradients through-the-thickness in multiply stacks [58]; the thick resin-rich interlayer might affect interply slip behaviour which in turns impacts the magnitude of wrinkles [59,60]. The effect of intra-ply sliding on the quality of impregnation of the final part will also have to be investigated [61,62].
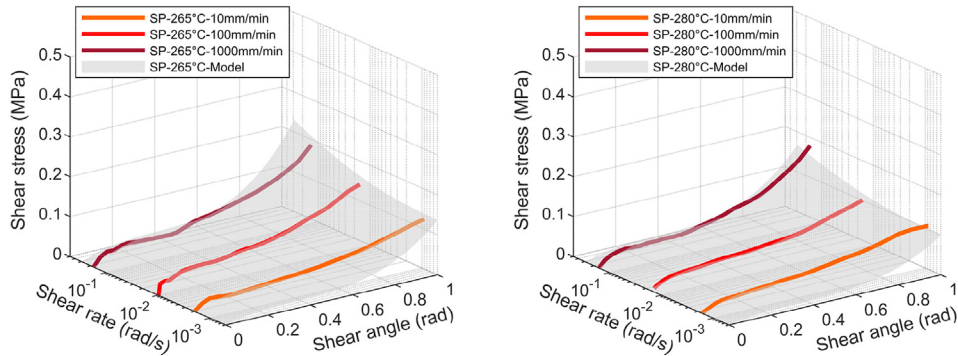

Fig. 16. Comparison between experimental data and model for semipreg specimens (SP) at 265°C (left) and 280°C (right). The grey surface represent the model prediction.
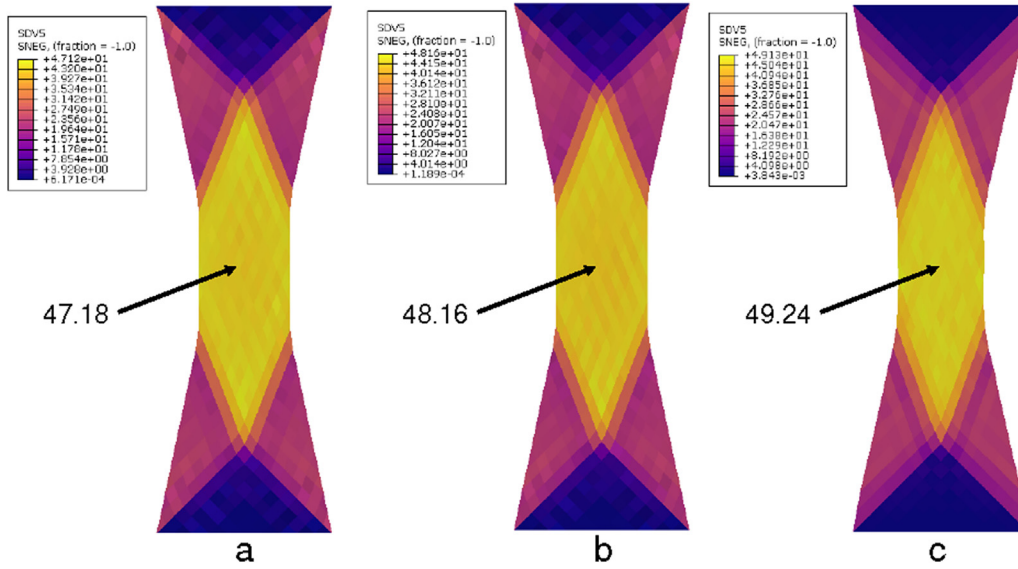
Fig. 18. Simulated shear angle for preconsolidated material (CS) at 1000 mm/min and: (a) 250°C, (b) 265°C, (c) 280°C, at 30 mm extension.
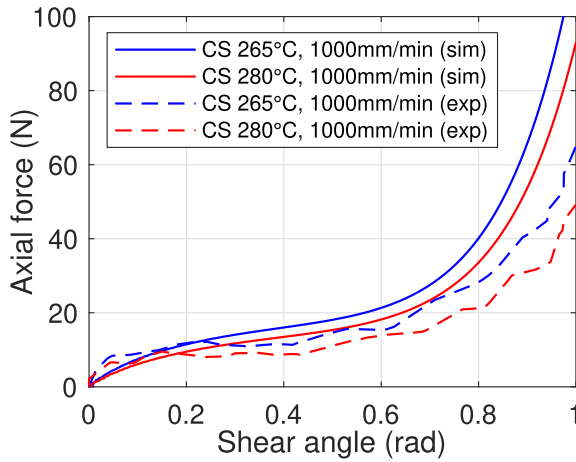

Fig. 19. Simulated and averaged experimental axial force for preconsolidated material (CS) at 1000 mm/min.
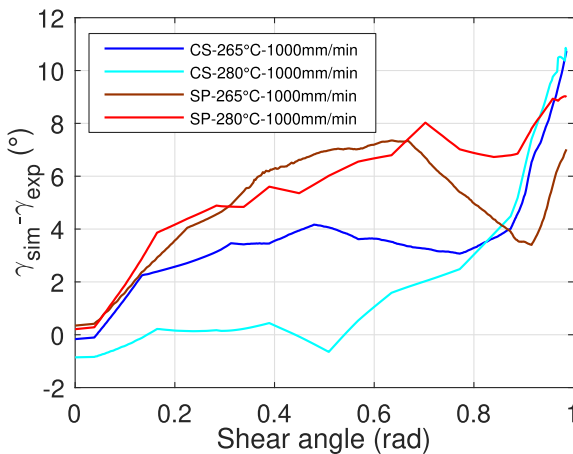

Fig. 20. Error between simulated and experimental shear angle at 1000 mm/min for preconsolidated (CS) and semipreg (SP).

7. Conclusion & outlook

The shear behaviour of a novel PA66/glass powder-impregnated woven semipreg was characterized using bias-extension tests in its as-received state and after a preconsolidation step. The influence of temperature and shear rate has been evaluated in a range representative of the thermoforming process. Results show a similar effect of the temperature in both material configurations, with an increase of the shear stiffness with decreasing temperature due to changes in the matrix viscosity. While the preconsolidated material shows increased shear stiffness at higher crosshead speeds, the semipreg exhibits a less significant dependence to shear rate. This behaviour is attributed to different friction mechanisms at the yarn crossover points: dry friction for the semipreg, compared to lubricated friction for the preconsolidated composite. Intra-ply slip mechanisms in semipregs leads to a characteristic pattern of dry zones and resin-rich boundaries. These modification to the local matrix volume fraction can affect the impregnation of the final part.

A hypoelastic approach was used to describe the mechanical behaviour of the material. The temperature and rate dependence observed experimentally were attributed to the in-plane shear term by a multiplicative decoupling model, based on phenomenological considerations. Simulations of the bias-extension tests were carried out. While the continuous approach was unable to reproduce inter-yarn sliding, the effects of temperature and rate were correctly replicated, with the model allowing for a correct prediction of both force and shear angle.

Acknowledgements

References

[1] Z. Yang, A. Bandivekar, Light-duty vehicle greenhouse gas and fuel economy standards, Tech. Rep., Int. Counc. Clean Transport. (2017).

[2] T. Renault, Developments in thermoplastic composites for automotive applications, Franco-British Symposium on Composite Materials, 2015 retrieved from https://uk.ambafrance.org/Summary-Franco-British-Symposium (Nov. 2018).

[3] M. Hou, Stamp forming of fabric-reinforced thermoplastic composites, Polym. Compos. 17 (4) (1996) 596–603, https://doi.org/10.1002/pc.10649.

[4] A.R. Offringa, Thermoplastic composites—rapid processing applications, Compos. Appl. Sci. Manuf. 27 (4) (1996) 329–336, https://doi.org/10.1016/1359-835x(95)00048-7.

[5] O. Diestel, J. Hausding, Pre-impregnated textile semi-finished products (prepregs),

Textile Materials for Lightweight Constructions, Springer Berlin Heidelberg, 2016, pp. 361–379, , https://doi.org/10.1007/978-3-662-46341-3-11.

[6] J. Faraj, N. Boyard, B. Pignon, J.-L. Bailleul, D. Delaunay, G. Orange, Crystallization kinetics of new low viscosity polyamides 66 for thermoplastic composites processing, Thermochim. Acta 624 (2016) 27–34, https://doi.org/10.1016/j.tca.2015.11.025.

[7] P. Boisse, N. Hamila, E. Guzman-Maldonado, A. Madeo, G. Hivet, F. dell'Isola, The bias-extension test for the analysis of in-plane shear properties of textile composite reinforcements and prepregs: a review, Int. J. Material Form. 10 (4) (2017) 473–492, https://doi.org/10.1007/s12289-016-1294-7.

[8] N. Svensson, R. Shishoo, M. Gilchrist, Manufacturing of thermoplastic composites from commingled yarns-A review, J. Thermoplast. Compos. Mater. 11 (1) (1998) 22–56, https://doi.org/10.1177/089270579801100102.

[9] N. Bernet, V. Michaud, P.E. Bourban, J.A. Manson, An impregnation model for the consolidation of thermoplastic composites made from commingled yarns, J. Compos. Mater. 33 (8) (1999) 751–772, https://doi.org/10.1177/002199839903300806.

[10] N. Bernet, V. Michaud, P.-E. Bourban, J.-A. Månson, Commingled yarn composites for rapid processing of complex shapes, Compos. Appl. Sci. Manuf. 32 (11) (2001) 1613–1626, https://doi.org/10.1016/s1359-835x(00)00180-9.

[11] U. Thomann, Direct Stamp Forming of Non-consolidated Carbon/thermoplastic Fibre Commingled Yarns, Ph.D. thesis, ETH Zürich (2003), https://doi.org/10.3929/ethz-a-004631034.

[12] U. Thomann, M. Sauter, P. Ermanni, A combined impregnation and heat transfer model for stamp forming of unconsolidated commingled yarn preforms, Compos. Sci. Technol. 64 (10–11) (2004) 1637–1651, https://doi.org/10.1016/j.compscitech.2003.12.002.

[13] D. Trudel-Boucher, B. Fisa, J. Denault, P. Gagnon, Experimental investigation of stamp forming of unconsolidated commingled E-glass/polypropylene fabrics, Compos. Sci. Technol. 66 (3–4) (2006) 555–570, https://doi.org/10.1016/j.compscitech.2005.05.036.

[14] M. Wakeman, L. Zingraff, P.-E. Bourban, J.-A. Månson, P. Blanchard, Stamp forming of carbon fibre/PA12 composites – a comparison of a reactive impregnation process and a commingled yarn system, Compos. Sci. Technol. 66 (1) (2006) 19–35, https://doi.org/10.1016/j.compscitech.2005.06.001.

[15] M. Connor, Consolidation Mechanisms and Interfacial Phenomena in Thermoplastic Powder Impregnated Composites, Ph.D. thesis Ecole Polytechnique Fédérale de Lausanne, 1995, https://doi.org/10.5075/epfl-thesis-1413.

[16] E. Guzman-Maldonado, N. Hamila, P. Boisse, J. Bikard, Thermomechanical analysis, modelling and simulation of the forming of pre-impregnated thermoplastics composites, Compos. Appl. Sci. Manuf. 78 (2015) 211–222, https://doi.org/10.1016/j.compositesa.2015.08.017.

[17] E. Guzman-Maldonado, N. Hamila, N. Naouar, G. Moulin, P. Boisse, Simulation of thermoplastic prepreg thermoforming based on a visco-hyperelastic model and a thermal homogenization, Mater. Des. 93 (2016) 431–442, https://doi.org/10.1016/j.matdes.2015.12.166.

[18] M. Machado, M. Fischlschweiger, Z. Major, A rate-dependent non-orthogonal constitutive model for describing shear behaviour of woven reinforced thermoplastic composites, Compos. Appl. Sci. Manuf. 80 (2016) 194–203, https://doi.org/10.1016/j.compositesa.2015.10.028.

[19] P. Harrison, M. Clifford, A. Long, Shear characterisation of viscous woven textile composites: a comparison between picture frame and bias extension experiments, Compos. Sci. Technol. 64 (10–11) (2004) 1453–1465, https://doi.org/10.1016/j.compscitech.2003.10.015.

[20] G. Lebrun, M.N. Bureau, J. Denault, Evaluation of bias-extension and picture-frame test methods for the measurement of intraply shear properties of PP/glass commingled fabrics, Compos. Struct. 61 (4) (2003) 341–352, https://doi.org/10.1016/s0263-8223(03)00057-6.

[21] B. Zhu, T. Yu, X. Tao, Large deformation and slippage mechanism of plain woven composite in bias extension, Compos. Appl. Sci. Manuf. 38 (8) (2007) 1821–1828, https://doi.org/10.1016/j.compositesa.2007.04.009.

[22] J. Cao, R. Akkerman, P. Boisse, J. Chen, H. Cheng, E. de Graaf, J. Gorczyca, P. Harrison, G. Hivet, J. Launay, W. Lee, L. Liu, S. Lomov, A. Long, E. de Luycker, F. Morestin, J. Padvoiskis, X. Peng, J. Sherwood, T. Stoilova, X. Tao, I. Verpoest, A. Willems, J. Wiggers, T. Yu, B. Zhu, Characterization of mechanical behavior of woven fabrics: experimental methods and benchmark results, Compos. Appl. Sci. Manuf. 39 (6) (2008) 1037–1053, https://doi.org/10.1016/j.compositesa.2008.02.016.

[23] Evolite XA1481 Technical Data Sheet, Solvay, 2012.

[24] S.R. Iyer, L.T. Drzal, Manufacture of powder-impregnated thermoplastic composites, J. Thermoplast. Compos. Mater. 3 (4) (1990) 325–355, https://doi.org/10.1177/089270579000300404.

[25] L.M. Dangora, C.J. Hansen, C.J. Mitchell, J.A. Sherwood, J.C. Parker, Challenges associated with shear characterization of a cross-ply thermoplastic lamina using picture frame tests, Compos. Appl. Sci. Manuf. 78 (2015) 181–190, https://doi.org/10.1016/j.compositesa.2015.08.015.

[26] X. Peng, J. Cao, Bias Extension Test Standard, Tech. Rep. Northwestern University, 2003.

[27] J. Schindelin, I. Arganda-Carreras, E. Frise, V. Kaynig, M. Longair, T. Pietzsch, S. Preibisch, C. Rueden, S. Saalfeld, B. Schmid, J.-Y. Tinevez, D.J. White, V. Hartenstein, K. Eliceiri, P. Tomancak, A. Cardona, Fiji: an open-source platform for biological-image analysis, Nat. Methods 9 (7) (2012) 676–682, https://doi.org/10.1038/nmeth.2019.

[28] J. Launay, G. Hivet, A.V. Duong, P. Boisse, Experimental analysis of the influence of tensions on in plane shear behaviour of woven composite reinforcements, Compos. Sci. Technol. 68 (2) (2008) 506–515, https://doi.org/10.1016/j.compscitech.2007.

[29] F. Härtel, P. Harrison, Evaluation of normalisation methods for uniaxial bias extension tests on engineering fabrics, Compos. Appl. Sci. Manuf. 67 (2014) 61–69, https://doi.org/10.1016/j.compositesa.2014.08.011.

[30] G. Hivet, E. Vidal-Sallé, P. Boisse, Analysis of the stress components in a textile composite reinforcement, J. Compos. Mater. 47 (3) (2012) 269–285, https://doi.org/10.1177/0021998312439222.

[31] Z. Dong, C. Sun, Testing and modeling of yarn pull-out in plain woven Kevlar fabrics, Compos. Appl. Sci. Manuf. 40 (12) (2009) 1863–1869, https://doi.org/10.1016/j.compositesa.2009.04.019.

[32] M. Machado, L. Murenu, M. Fischlschweiger, Z. Major, Analysis of the thermo-mechanical shear behaviour of woven-reinforced thermoplastic-matrix composites during forming, Compos. Appl. Sci. Manuf. 86 (2016) 39–48, https://doi.org/10.1016/j.compositesa.2016.03.032.

[33] S. Haanappel, R. ten Thije, U. Sachs, B. Rietman, R. Akkerman, Formability analyses of uni-directional and textile reinforced thermoplastics, Compos. Appl. Sci. Manuf. 56 (2014) 80–92, https://doi.org/10.1016/j.compositesa.2013.09.009.

[34] D. Durville, Simulation of the mechanical behaviour of woven fabrics at the scale of fibers, Int. J. Material Form. 3 (S2) (2010) 1241–1251, https://doi.org/10.1007/s12289-009-0674-7.

[35] P. Badel, E. Vidal-Sallé, E. Maire, P. Boisse, Simulation and tomography analysis of textile composite reinforcement deformation at the mesoscopic scale, Compos. Sci. Technol. 68 (12) (2008) 2433–2440, https://doi.org/10.1016/j.compscitech.2008.04.038.

[36] R. ten Thije, R. Akkerman, J. Huétink, Large deformation simulation of anisotropic material using an updated Lagrangian finite element method, Comput. Methods Appl. Mech. Eng. 196 (33–34) (2007) 3141–3150, https://doi.org/10.1016/j.cma.2007.02.010.

[37] N. Hamila, P. Boisse, F. Sabourin, M. Brunet, A semi-discrete shell finite element for textile composite reinforcement forming simulation, Int. J. Numer. Methods Eng. 79 (12) (2009) 1443–1466, https://doi.org/10.1002/nme.2625.

[38] P. Boisse, N. Hamila, E. Vidal-Sallé, F. Dumont, Simulation of wrinkling during textile composite reinforcement forming. Influence of tensile, in-plane shear and bending stiffnesses, Compos. Sci. Technol. 71 (5) (2011) 683–692, https://doi.org/10.1016/j.compscitech.2011.01.011.

[39] R. Pierce, B. Falzon, M. Thompson, R. Boman, Implementation of a non-orthogonal constitutive model for the finite element simulation of textile composite draping, Appl. Mech. Mater. 553 (2014) 76–81 https://doi.org/10.4028/www.scientific.net/amm.553.76.

[40] M. Khan, T. Mabrouki, E. Vidal-Sallé, P. Boisse, Numerical and experimental analyses of woven composite reinforcement forming using a hypoelastic behaviour. Application to the double dome benchmark, J. Mater. Process. Technol. 210 (2) (2010) 378–388, https://doi.org/10.1016/j.jmatprotec.2009.09.027.

[41] X. Peng, J. Cao, A continuum mechanics-based non-orthogonal constitutive model for woven composite fabrics, Compos. Appl. Sci. Manuf. 36 (6) (2005) 859–874, https://doi.org/10.1016/j.compositesa.2004.08.008.

[42] M.H. Kashani, A. Rashidi, B. Crawford, A. Milani, Analysis of a two-way tension-shear coupling in woven fabrics under combined loading tests: global to local transformation of non-orthogonal normalized forces and displacements, Compos. Appl. Sci. Manuf. 88 (2016) 272–285, https://doi.org/10.1016/j.compositesa.2016.06.004.

[43] M. Komeili, A. Milani, On effect of shear-tension coupling in forming simulation of woven fabric reinforcements, Compos. B Eng. 99 (2016) 17–29, https://doi.org/10.1016/j.compositesb.2016.05.004.

[44] G. Cowper, P. Symonds, Strain Hardening and Strain-Rate Effects In the Impact Loading of Cantilever Beams, Tech. Rep. Brown University, 1957.

[45] R. Waltz, J. Morales, J. Nocedal, D. Orban, An interior algorithm for nonlinear optimization that combines line search and trust region steps, Math. Program. 107 (3) (2005) 391–408, https://doi.org/10.1007/s10107-004-0560-5.

[46] N. Hamila, P. Boisse, Locking in simulation of composite reinforcement deformations. Analysis and treatment, Compos. Appl. Sci. Manuf. 53 (2013) 109–117, https://doi.org/10.1016/j.compositesa.2013.06.001.

[47] S. Lomov, P. Boisse, E. Deluycker, F. Morestin, K. Vanclooster, D. Vandepitte, I. Verpoest, A. Willems, Full-field strain measurements in textile deformability studies, Compos. Appl. Sci. Manuf. 39 (8) (2008) 1232–1244, https://doi.org/10.1016/j.compositesa.2007.09.014.

[48] H. Bersee, L. Robroek, The role of the thermoplastic matrix in forming processes of composite materials, Compos. Manuf. 2 (3–4) (1991) 217–222, https://doi.org/10.1016/0956-7143(91)90143-5.

[49] A. Johnson, Rheological model for the forming of fabric-reinforced thermoplastic sheets, Compos. Manuf. 6 (3–4) (1995) 153–160, https://doi.org/10.1016/0956-7143(95)95006-k.

[50] R. ten Thije, R. Akkerman, M. Ubbink, L. van der Meer, A lubrication approach to friction in thermoplastic composites forming processes, Compos. Appl. Sci. Manuf. 42 (8) (2011) 950–960, https://doi.org/10.1016/j.compositesa.2011.03.023.

[51] L. Liu, J. Chen, J.L. Gorczyca, J.A. Sherwood, Modeling of friction and shear in thermostamping of composites - Part II, J. Compos. Mater. 38 (21) (2004) 1931–1947, https://doi.org/10.1177/0021998304048417.

[52] J.L. Gorczyca, J.A. Sherwood, L. Liu, J. Chen, Modeling of friction and shear in thermostamping of composites - Part I, J. Compos. Mater. 38 (21) (2004) 1911–1929, https://doi.org/10.1177/0021998304048416.

[53] L. Liu, J. Chen, B. Zhu, T. Yu, X. Tao, J. Cao, The yarn-to-yarn friction of woven fabrics, Proceedings of the 9th ESAFORM Conference, 2006.

[54] B. Cornelissen, B. Rietman, R. Akkerman, Frictional behaviour of high performance fibrous tows: friction experiments, Compos. Appl. Sci. Manuf. 44 (2013) 95–104, https://doi.org/10.1016/j.compositesa.2012.08.024.

[55] U. Sachs, R. Akkerman, K. Fetfatsidis, E. Vidal-Sallé, J. Schumacher, G. Ziegmann, S. Allaoui, G. Hivet, B. Maron, K. Vanclooster, S. Lomov, Characterization of the dynamic friction of woven fabrics: experimental methods and benchmark results, Compos. Appl. Sci. Manuf. 67 (2014) 289–298, https://doi.org/10.1016/j.compositesa.2014.08.026.

[56] L. Montero, S. Allaoui, G. Hivet, Characterisation of the mesoscopic and macroscopic friction behaviours of glass plain weave reinforcement, Compos. Appl. Sci. Manuf. 95 (2017) 257–266, https://doi.org/10.1016/j.compositesa.2017.01.022.

[57] R. Akkerman, A continuum mechanics analysis of shear characterisation methods, Compos. Appl. Sci. Manuf. 109 (2018) 131–140, https://doi.org/10.1016/j.compositesa.2018.02.036.

[58] T. Baumard, O. De Almeida, G. Menary, Y. Le Maoult, F. Schmidt, J. Bikard, Determination of thermal contact conductance in vacuum-bagged thermoplastic prepreg stacks using infrared thermography, AIP Conference Proceedings 1769, Author(s), 2016, https://doi.org/10.1063/1.4963511.

[59] Q. Chen, P. Boisse, C.H. Park, A. Saouab, J. Bréard, Intra/inter-ply shear behaviors of continuous fiber reinforced thermoplastic composites in thermoforming processes, Compos. Struct. 93 (7) (2011) 1692–1703, https://doi.org/10.1016/j.compstruct.2011.01.002.

[60] S. Allaoui, C. Cellard, G. Hivet, Effect of inter-ply sliding on the quality of multilayer interlock dry fabric preforms, Compos. Appl. Sci. Manuf. 68 (2015) 336–345, https://doi.org/10.1016/j.compositesa.2014.10.017.

[61] L. Ye, V. Klinkmuller, K. Friedrich, Impregnation and consolidation in composites made of GF/PP powder impregnated bundles, J. Thermoplast. Compos. Mater. 5 (1) (1992) 32–48, https://doi.org/10.1177/089270579200500103.

[62] M. Connor, S. Toll, J.A.E. Månson, A.G. Gibson, A model for the consolidation of aligned thermoplastic powder impregnated composites, J. Thermoplast. Compos. Mater. 8 (2) (1995) 138–162, https://doi.org/10.1177/089270579500800201.